Role of long waves in the stability of the plane wake

Stefania Scarsoglio and Daniela Tordella*

Dipartimento di Ingegneria Aeronautica e Spaziale, Politecnico di Torino, 10129 Torino, Italy

William O. Criminale

Department of Applied Mathematics, University of Washington, Seattle, Washington 98195-2420, USA
(Received 8 July 2009; revised manuscript received 27 January 2010; published 29 March 2010)

This work is directed toward investigating the fate of three-dimensional long perturbation waves in a plane incompressible wake. The analysis is posed as an initial-value problem in space. More specifically, input is made at an initial location in the downstream direction and then tracing the resulting behavior further downstream subject to the restriction of finite kinetic energy. This presentation follows the outline given by Criminale and Drazin [W. O. Criminale and P. G. Drazin, Stud. Appl. Math. **83**, 123 (1990)] that describes the system in terms of perturbation vorticity and velocity. The analysis is based on large scale waves and expansions using multiscales and multitimes for the partial differential equations. The multiscaling is based on an approach where the small parameter is linked to the perturbation property independently from the flow control parameter. Solutions of the perturbative equations are determined numerically after the introduction of a regular perturbation scheme analytically deduced up to the second order. Numerically, the complete linear system is also integrated. Since the results relevant to the complete problem are in very good agreement with the results of the first-order analysis, the numerical solution at the second order was deemed not necessary. The use for an arbitrary initial-value problem will be shown to contain a wealth of information for the different transient behaviors associated to the symmetry, angle of obliquity, and spatial decay of the long waves. The amplification factor of transversal perturbations never presents the trend—a growth followed by a long damping—usually seen in waves with wave number of order one or less. Asymptotical instability is always observed.

I. INTRODUCTION

The traditional investigation of stability of shear flows is cast as a linear initial-value perturbation problem. In principle, save for the additional complexity of necessitating three space dimensions as well as time, this is done by means of a Laplace transform in time. Once the boundary conditions have been satisfied, the stability or non stability is found. Further, depending upon the mean shear flow that is being investigated, the causes are determined. No attention is given to any specific input or the effect of various physics. Moreover, little attention was given to early period dynamics, see, for example, Grosch and Salwen [1] and Salwen and Grosch [2]. These authors showed that there can be early time growth of a perturbation even if there is damping for long time. In short, a branch cut can be present as well as any pole when inverting the Laplace transform. Next, from the laboratory, interest turned to spatial growth or decay after an input at an initial location rather than the temporal behavior. This construction creates new difficulties but they are not insurmountable [3,4]. Still, just as in the temporal problem, no specific initial input has been examined. Regardless of the framework, it has been known since the first results of stability theory that the value of the wave number that comes into the analytical framework (due to Fourier decomposition in the variables in the plane that is perpendicular to the mean flow) is small in the regions where there is instability, in short, long waves. Such a result provides a sound means for the analysis and examination of a specific initial input. This is true whether posed as a temporal or spatial initial-value problem. It further provides a means to investigate interaction, the early period and a way to suppress any growth at the early period or location. In 1962 a study about the instability to long waves of unbounded parallel inviscid flow was given by Drazin and Howard [5]. Using the normal mode analysis, they found that there is a finite number of different modes unstable to long waves, essentially one for each relative maximum or minimum of the velocity profile. Healey [6] considered long waves for investigating spatial instability of the rotating-disk boundary layer, and by means of an analytic theory in the inviscid long wave limit, he obtained an explicit expression for the growth rate in terms of basic flow parameters.

Large or long waves have now been used in full nonlinear simulations. For example, Ryzkov and Shevtsova [7] focused on convective instability in multicomponent fluids, showing by means of both linear stability analysis and nonlinear numerical calculations that the instability is caused by the interplay between the basic flow and the concentration waves which have a long scale in a vertical direction. And Barros and Choi [8] considered the inhibition of the shear instability that can be induced by large amplitude internal solitary waves traveling in a two-layer flow with a top free surface. For large eddy simulations in turbulence see [9] or [10] among many others.

The analysis in the present work is based on large scale waves and expansions using multiscales and multitimes for the partial differential equations. The multiscale is based on

_____

*daniela.tordella@polito.it

an approach where the small parameter is linked to the perturbation property independently from the flow control parameter. In fact, the perturbation scheme is based on the introduction of a small parameter which is the wave number k in the limit $k \to 0$ and is analytically determined to the second order. The perturbative equations used follow the formulation given by Criminale and Drazin [11] that describes the system in terms of perturbation vorticity and velocity. Numerically, the complete linear system has also been integrated for the nonparallel base flow. What results is an extension of a previous work based on a locally near parallel assumption [12]. The formulation of the linear perturbation initial-value problem is presented in Sec. II. Results are in Sec. III. Conclusions follow in Sec. IV.

II. FORMULATION

By exciting the plane wake flow $\{\mathbf{U} = [U(x, y; \mathrm{Re}), V(x, y; \mathrm{Re})]\}$ with small arbitrary three-dimensional perturbations, the continuity and Navier-Stokes equations for the perturbed system linearized with respect to small oscillations are given by

$$\frac{\partial \tilde{u}}{\partial x} + \frac{\partial \tilde{v}}{\partial y} + \frac{\partial \tilde{w}}{\partial z} = 0, \tag{1}$$

$$\frac{\partial \tilde{u}}{\partial t} + \tilde{u}\frac{\partial U}{\partial x} + U\frac{\partial \tilde{u}}{\partial x} + \tilde{v}\frac{\partial U}{\partial y} + V\frac{\partial \tilde{u}}{\partial y} + \frac{\partial \tilde{p}}{\partial x} = \frac{1}{\mathrm{Re}}\nabla^2\tilde{u}, \tag{2}$$

$$\frac{\partial \tilde{v}}{\partial t} + \tilde{u}\frac{\partial V}{\partial x} + U\frac{\partial \tilde{v}}{\partial x} + \tilde{v}\frac{\partial V}{\partial y} + V\frac{\partial \tilde{v}}{\partial y} + \frac{\partial \tilde{p}}{\partial y} = \frac{1}{\mathrm{Re}}\nabla^2\tilde{v}, \tag{3}$$

$$\frac{\partial \tilde{w}}{\partial t} + U\frac{\partial \tilde{w}}{\partial x} + V\frac{\partial \tilde{w}}{\partial y} + \frac{\partial \tilde{p}}{\partial z} = \frac{1}{\mathrm{Re}}\nabla^2\tilde{w}, \tag{4}$$

where $[\tilde{u}(x, y, z, t), \tilde{v}(x, y, z, t),$ and $\tilde{w}(x, y, z, t)]$ and $\tilde{p}(x, y, z, t)$ are the components of the perturbation velocity and pressure, respectively.

The independent spatial variables z and y are defined from $-\infty$ to $+\infty$ and x are defined from 0 to $+\infty$. All physical quantities are normalized with respect to the free stream velocity U_f, the body scale D, and the density ρ. The Reynolds number is defined as $\mathrm{Re} = U_f D / \nu$, where ν is the kinematic viscosity.

The two-dimensional wake is a thin free flow that can be schematized as shown in Fig. 1. Leaving aside the near field, that is highly non parallel since it hosts the two symmetric countercirculating vortices that constitute the separation region, the intermediate and long term wake is a near parallel flow. The wake slowly becomes thicker according to a law which, at first order, scales as $(x/\mathrm{Re})^{1/2}$. As representation of this steady subcritical flow we consider the asymptotic expansion solution in inverse powers of x obtained in [13]. In particular, we consider the intermediate far field well represented by a section placed near $x = x_0 = 10$ and build the basic flow by freezing it at this longitudinal station. In so doing, the basic flow is parameterized through the downstream station x_0 and the Reynolds number Re $\{\mathbf{U} = [U(y; x_0, \mathrm{Re}), V(y; x_0, \mathrm{Re})]\}$. It is thus homogeneous
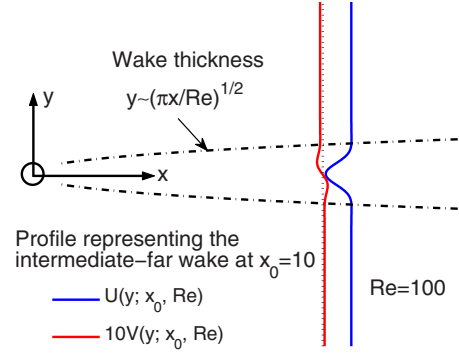

FIG. 1. (Color online) Base flow sketch. The base flow has been chosen in order to be an acceptable representation of the intermediate-far field. To this aim we build a homogeneous field in x, z by using the information associated to a section, x_0, placed in the intermediate region, $x \in [5, 30]$. In the sketch the longitudinal and transversal profiles at Re$=100$ are frozen at $x_0 = 10$ (note that the transversal velocity V is multiplied by a factor of ten). The base flow $[U(y; x_0, \mathrm{Re}), V(y; x_0, \mathrm{Re})]$ is thus a slightly non parallel flow homogeneous in x, z, which makes it possible to Laplace transform the perturbative equations in x and to Fourier transform them in z.

in x and z. As such, the long waves that are the main subject of this paper are valid.

The explicit expressions of the base flow longitudinal and transversal components are

$$U(y; x_0, \mathrm{Re}) = \phi_0 + \phi_1 x_0^{-1/2} + \phi_2 x_0^{-1} + \phi_3 x_0^{-3/2}, \tag{5}$$

$$V(y; x_0, \mathrm{Re}) = \chi_0 + \chi_1 x_0^{-1/2} + \chi_2 x_0^{-1} + \chi_3 x_0^{-3/2}. \tag{6}$$

The coefficients $\phi_i = \phi_i(y; x_0, \mathrm{Re})$ and $\chi_i = \chi_i(y; x_0, \mathrm{Re})$ of this expansion up to $i = 3$ are given in Appendix A. Figure 2 displays the intermediate wake profile for which there exists a comparison based on laboratory and numerical simulation results, see also [13–16].

It should be noted that when using such a kind of representation the base flow nonparallelism is considered and allows for the effect of the lateral entrainment to be obtained [16]. However, in this paper a fixed location x_0 of the intermediate wake is considered since in this region absolute instability pockets have been found by recent modal analyses [17,18]. The term intermediate is used in the general sense as
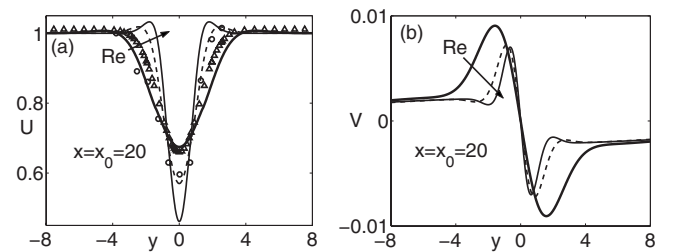

FIG. 2. Example of velocity profiles in the intermediate wake at the downstream station $x = x_0 = 20$. (a) Longitudinal velocity U and (b) transversal velocity V. Continuous curves: analytical solutions (Re$=20$, 60, and 100) by Tordella and Belan (2003) [13], triangles: numerical results (Re$=34$) by Berrone (2001) [14], and circles: laboratory data (Re$=34$) by Kovasznay (1948) [15].

that given by Barenblatt [19]: "… intermediate asymptotics are self-similar or near-similar solutions of general problems valid for times and distances from boundaries large enough for the influence of the fine details of the initial or boundary conditions to be insignificant but small enough that the system is far from the ultimate equilibrium state…." The distance beyond which the intermediate region is assumed to begin varies from eight to four diameters D for $\mathrm{Re} \in [20,40]$ [13].

By combining the momentum Eqs. (2)–(4) to eliminate the pressure, the resulting governing equations become

$$
\frac{\partial \nabla^2 \widetilde{v}}{\partial t} = -\left[U\frac{\partial}{\partial x} + V\frac{\partial}{\partial y} - \frac{1}{\mathrm{Re}}\nabla^2 \right]\nabla^2\widetilde{v} - \left[a\frac{\partial}{\partial x} + b \right]\widetilde{u}
$$
$$
- \left[\frac{\partial \Omega_z}{\partial y}\frac{\partial}{\partial x} + c(y) \right]\widetilde{v} + a\frac{\partial \widetilde{w}}{\partial z} + \frac{\partial V}{\partial y}\frac{\partial \widetilde{\omega}_x}{\partial z} - e\frac{\partial \widetilde{\omega}_y}{\partial z}
$$
$$
- \left[d\frac{\partial}{\partial x} + e\frac{\partial}{\partial y} \right]\widetilde{\omega}_z, \qquad (7)
$$

$$
\frac{\partial \widetilde{\omega}_y}{\partial t} = -\left[U\frac{\partial}{\partial x} + V\frac{\partial}{\partial y} + d - \frac{1}{\mathrm{Re}}\nabla^2 \right]\widetilde{\omega}_y - \frac{\partial U}{\partial y}\frac{\partial \widetilde{v}}{\partial z} + e\frac{\partial \widetilde{w}}{\partial y}, \qquad (8)
$$

where $(\widetilde{\omega}_x, \widetilde{\omega}_y, \widetilde{\omega}_z)$ is the perturbation vorticity field, $\Omega_z = (\frac{\partial V}{\partial x} - \frac{\partial U}{\partial y})|_{x=x_0}$ is the mean vorticity in the spanwise direction, and the coefficients a, b, c, d, e are the spatial derivatives of the base flow vorticity and velocity at x_0, namely,

$$
a = \left.\frac{\partial \Omega_z}{\partial x}\right|_{x=x_0}, \quad b = \left.\frac{\partial^2 \Omega_z}{\partial x^2}\right|_{x=x_0}, \quad c(y) = \left.\frac{\partial^2 \Omega_z}{\partial x\,\partial y}\right|_{x=x_0},
$$
$$
d = \left.\frac{\partial U}{\partial x}\right|_{x=x_0}, \quad e = \left.\frac{\partial V}{\partial x}\right|_{x=x_0}.
$$

By introducing the quantity $\widetilde{\Gamma}$, which is defined by

$$
\nabla^2\widetilde{v} = \widetilde{\Gamma}, \qquad (9)
$$

we obtain three coupled Eqs. (7)–(9). Equations (7) and (8) are the Orr-Sommerfeld and Squire equations, respectively, from the classical linear stability analysis for three-dimensional disturbances. From kinematics, the relation

$$
\widetilde{\Gamma} = \frac{\partial \widetilde{\omega}_z}{\partial x} - \frac{\partial \widetilde{\omega}_x}{\partial z} \qquad (10)
$$

physically links the perturbation vorticity components in the x and z directions ($\widetilde{\omega}_x$ and $\widetilde{\omega}_z$, respectively) and the perturbed velocity field. By combining Eqs. (7) and (9) then

$$
\frac{\partial \widetilde{\Gamma}}{\partial t} = -\left[U\frac{\partial}{\partial x} + V\frac{\partial}{\partial y} - \frac{1}{\mathrm{Re}}\nabla^2 \right]\widetilde{\Gamma} - \left[a\frac{\partial}{\partial x} + b \right]\widetilde{u} - \left[\frac{\partial \Omega_z}{\partial y}\frac{\partial}{\partial x} \right.
$$
$$
\left. + c(y) \right]\widetilde{v} + a\frac{\partial \widetilde{w}}{\partial z} + \frac{\partial V}{\partial y}\frac{\partial \widetilde{\omega}_x}{\partial z} - e\frac{\partial \widetilde{\omega}_y}{\partial z} - \left[d\frac{\partial}{\partial x} + e\frac{\partial}{\partial y} \right]\widetilde{\omega}_z, \qquad (11)
$$

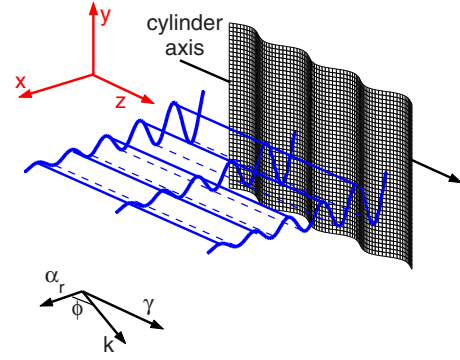which, together with Eqs. (8) and (9), fully describes the perturbed system. Since seven unknown quantities

FIG. 3. (Color online) Perturbation geometry scheme.

$(\widetilde{u}, \widetilde{v}, \widetilde{w}, \widetilde{\omega}_x, \widetilde{\omega}_y, \widetilde{\omega}_z, \widetilde{\Gamma})$ are involved in the above Eqs. (8), (9), and (11), the perturbation vorticity definition and the continuity equation

$$
\underline{\widetilde{\omega}} = \nabla \times \underline{\widetilde{u}}, \qquad (12)
$$

$$
\nabla \cdot \underline{\widetilde{u}} = 0, \qquad (13)
$$

link the perturbative system of Eqs. (8), (9), and (11).

For every dependent variable, we perform a combined spatial Laplace-Fourier decomposition in the x and z directions defined by

$$
\hat{g}(y,t;\alpha,\gamma) = \int_{-\infty}^{+\infty}\int_0^{+\infty} \widetilde{g}(x,y,z,t)e^{-i\alpha x - i\gamma z}\,dx\,dz,
$$

where $\widetilde{g}$ is the general dependent variable, α, which is the longitudinal wave number, is complex ($\alpha = \alpha_r + i\alpha_i$), and γ, which is the transversal wave number, is real. By adopting the velocity-vorticity formulation [3,11], the governing Eqs. (8), (9), and (11) can now be written as

$$
\frac{\partial^2 \hat{v}}{\partial y^2} - [k^2 - \alpha_i^2 + 2ik\cos(\phi)\alpha_i]\hat{v} = \hat{\Gamma}, \qquad (14)
$$

$$
\frac{\partial \hat{\Gamma}}{\partial t} = G\hat{\Gamma} + H\hat{v} + K\hat{\omega}_y, \qquad (15)
$$

$$
\frac{\partial \hat{\omega}_y}{\partial t} = L\hat{\omega}_y + M\hat{v}, \qquad (16)
$$

where $\phi = \tan^{-1}(\gamma/\alpha_r)$ is the perturbation angle of obliquity with respect to the x-y physical plane, $k = \sqrt{\alpha_r^2 + \gamma^2}$ is the polar wave number, α_i is the imaginary part of the complex longitudinal wave number, $\hat{\omega}_y$ is the transversal component of the perturbation vorticity, and $\hat{\Gamma}$ is the vorticity component in the oblique direction which is defined as $\hat{\Gamma} = i(\alpha\hat{\omega}_z - \gamma\hat{\omega}_x)$. In Fig. 3 the three-dimensional perturbative geometry scheme is shown.

In order to have a finite perturbation kinetic energy, α_i can only assume non-negative values. In so doing, we allow for perturbative waves that can spatially decay ($\alpha_i > 0$) or remain constant in amplitude ($\alpha_i = 0$). In the following, α_i is called spatial damping rate. It should be pointed out that the
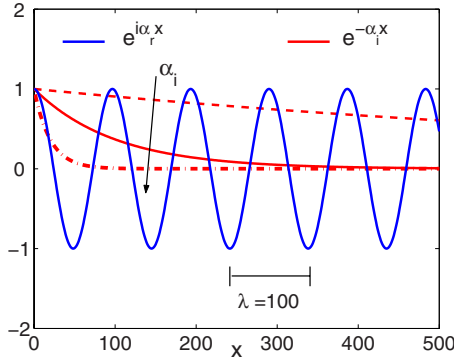
FIG. 4. (Color online) The wave spatial evolution in the x direction for $k = \alpha_r = 0.05$ and $\alpha_i = 0.1, 0.01, 0.001$.

present analysis is not the standard eigenvalue problem where poles result. Here, in fact, the spatial damping rate α_i is a parameter and, as such, should be simply imposed. The magnitude of the spatial damping rate can vary in order to describe a physically meaningful damping of the perturbative wave in the x direction (disturbances immediately damped to zero are not allowed). According to this and since long waves ($k \sim 10^{-1}, 10^{-2}$) are considered, α_i is non-negative and at maximum $\sim 10^{-1}$ (see Fig. 4). Symbols G, H, K, L, and M represent ordinary differential operators, written in the form $G = G(y; x_0, k, \phi, \alpha_i, \text{Re})$, and similarly for H, K, L, and M, since they are functions of y and are parametrized through the fixed longitudinal station x_0, the polar wave number k, the angle of obliquity ϕ, the spatial damping rate α_i, and the Reynolds number Re. All these operators are explicitly given in Appendix B.

Equations (14)–(16) require proper initial and boundary conditions in order to be solved. As far as the boundary conditions are concerned, among all solutions, those whose perturbation velocity field vanishes in the free stream are sought. The initial conditions are necessary for $\hat{\Gamma}$ and $\hat{\omega}_y$. As far as the initial conditions for $\hat{\Gamma}$ are concerned, according to Eq. (6), they can be shaped in terms of set of functions in the L^2 Hilbert space via the variable $\hat{v}$, which is here represented by the trigonometric system

$$\hat{v}(0, y) = e^{-y^2} \cos(y), \quad \hat{v}(0, y) = e^{-y^2} \sin(y),$$

for the symmetric and the asymmetric perturbations, respectively. This trigonometrical system is a Schauder basis in each space $L^p[0, 1]$ for $1 < p < \infty$. The transversal vorticity $\hat{\omega}_y$ is instead taken initially equal to zero in the y domain, in order to directly observe the net contribution of three dimensionality on its temporal evolution. However, it can be demonstrated that the eventual introduction of an initial transversal vorticity does not substantially affect the perturbation temporal evolution.

In the stability analysis of spatially developing flows, different scales can be determined. Usually, long and slow scale, related to the slow base flow evolution, as well as short and fast scales linked to the disturbance dynamics, can be defined. However, it should be noticed that in some flow configurations, long waves can be destabilizing. Examples of

this behavior are the two-dimensional Blasius boundary layer, the three-dimensional cross-flow boundary layer, as well as the free shear flows. In such instances, the perturbation wave number is less than $O(1)$ where instability occurs. Thus, a regular perturbation scheme can be adopted, defining the polar wave number k as the small parameter [20,21]. It should be noted that by using such a long-wave expansion, the x-scale length of the perturbations is comparable to the x-scale length of the base flow. Indeed, we only consider the intermediate and far wake sections, where the flow slowly evolves in the longitudinal direction. Thus the near wake is not taken into account. In synthesis, the scale of the intermediate wake is of the order $x_0 \sim 10^1$, and the scale of the long perturbative waves is $\lambda = 2\pi/k \sim 10^1, 10^2$.

Two spatial scales, a short one, y, and a long one, $Y = ky$, are defined. For the temporal dynamics, three temporal scales, the fast one, t, and the slow ones, $\tau = kt$ and $T = k^2 t$, can be identified. The perturbation quantities $(\hat{v}, \hat{\Gamma}, \hat{\omega}_y)$ are now function of y, Y, t, τ, T, expressed as $\hat{\Gamma} = \hat{\Gamma}(y, Y, t, \tau, T; k, \phi, \alpha_i)$, and similarly for $\hat{v}$ and $\hat{\omega}_y$, and can be expanded as

$$\hat{v} = \hat{v}_0 + k\hat{v}_1 + k^2 \hat{v}_2 + \cdots,$$

$$\hat{\Gamma} = \hat{\Gamma}_0 + k\hat{\Gamma}_1 + k^2 \hat{\Gamma}_2 + \cdots,$$

$$\hat{\omega}_y = \hat{\omega}_{y0} + k\hat{\omega}_{y1} + k^2 \hat{\omega}_{y2} + \cdots. \quad (17)$$

Initial conditions at order $O(1)$ are defined as in the full linear problem, while at higher orders $[O(k), O(k^2), \ldots]$ are equal to zero. Boundary conditions remain as stated in the full linear problem. Substituting relations (17) in the full linear system [Eqs. (14)–(16)], the following ordered hierarchy of equations, expressed up to $O(k)$, result and are the following:

(i) Order $O(1)$;

$$\frac{\partial^2 \hat{v}_0}{\partial y^2} + \alpha_i^2 \hat{v}_0 = \hat{\Gamma}_0, \quad (18)$$

$$\frac{\partial \hat{\Gamma}_0}{\partial t} - G_0 \hat{\Gamma}_0 - H_0 \hat{v}_0 = 0, \quad (19)$$

$$\frac{\partial \hat{\omega}_{y0}}{\partial t} - L_0 \hat{\omega}_{y0} = 0. \quad (20)$$

(ii) Order $O(k)$;

$$\frac{\partial^2 \hat{v}_1}{\partial y^2} + \alpha_i^2 \hat{v}_1 = -2 \frac{\partial^2 \hat{v}_0}{\partial y \partial Y} + 2i \cos(\phi) \alpha_i \hat{v}_0 + \hat{\Gamma}_1, \quad (21)$$

$$\frac{\partial \hat{\Gamma}_1}{\partial t} - G_0 \hat{\Gamma}_1 - H_0 \hat{v}_1 = -\frac{\partial \hat{\Gamma}_0}{\partial \tau} + G_1 \hat{\Gamma}_0 + H_1 \hat{v}_0 + K_1 \hat{\omega}_{y0},$$
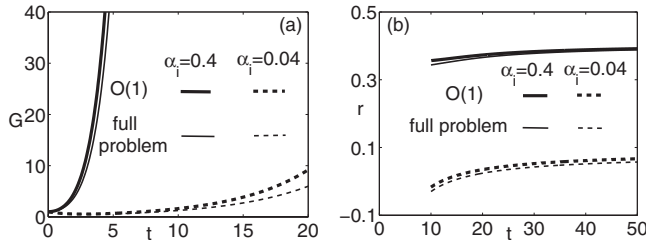
$$(22)$$

FIG. 5. Effects of the spatial damping rate α_i. (a) The amplification factor G and (b) the temporal growth rate r as function of time. Comparison between multiscale $O(1)$ (thick curves) and full problem (thin curves). Re=50, k=0.03, $\phi=\pi/4$, x_0=12, asymmetric initial condition, and α_i=0.04, 0.4.

$$\frac{\partial \hat{\omega}_{y1}}{\partial t} - L_0 \hat{\omega}_{y1} = -\frac{\partial \hat{\omega}_{y0}}{\partial \tau} + L_1 \hat{\omega}_{y0} + M_1 \hat{v}_0. \tag{23}$$

Operators $G_0 = G_0(y; x_0, \phi, \alpha_i, \text{Re})$ as well as H_0 and L_0 are functions of the short scale y only. Operators $G_1 = G_1(y, Y; x_0, \phi, \alpha_i, \text{Re})$ as well as H_1, K_1, L_1, and M_1 are function of both the short scale y as well as the long scale Y. These operators are explicitly given in Appendix B.

A comment concerning the role of α_i is needed. Equations (10)–(15) above are obtained for the case where $\alpha_i > 0$. It can be observed (see Appendix B) that if $\alpha_i = 0$, the $O(1)$ operators H_0, L_0 (but also the $O(k)$ operators H_1, L_1, M_1, and N_1) are singular. It is possible to verify that if $\alpha_i = 0$ the disturbances initially imposed remain constant as time passes and reach, in the end, an asymptotic condition of marginal stability. This fact is deduced by considering Eq. (18). For $\alpha_i = 0$, the homogeneous solution assumes the expression $\hat{v}_{0h} = c_1 + c_2 y$. Since the perturbation velocity field has to vanish in the free stream, $c_1 = 0$ and $c_2 = 0$. Thus $\hat{v}_0$ and therefore $\hat{\Gamma}_0$ vanish as well. This means that, in Eq. (19), $\frac{\partial \hat{\Gamma}_0}{\partial t} = 0$ so that there is no temporal evolution for $\hat{\Gamma}_0$. Since the transversal vorticity $\hat{\omega}_{y0}$ is initially taken as zero, then in Eq. (20), $\frac{\partial \hat{\omega}_{y0}}{\partial t} = 0$, and thus, also for the transversal vorticity, there is no temporal evolution. The complete problem is defined for $\alpha_i = 0$ and, for this value of α_i, it does not necessarily show a condition of marginal stability (e.g., see Fig. 6 in the following). However, it is possible to see that the multiscaling limit for $\alpha_i \rightarrow 0$ well approximates the complete problem: cf. Figs. 5 and 6. When $\alpha_i = 0$, the multiscaling presents a discontinuity since it has a right limit different from the value shown at $\alpha_i = 0$.

Order $O(1)$ is the more important approximation of the perturbative analysis and its formal expression is simplified with respect to the complete problem. Numerically, the complete linear system was also integrated. Since the results relevant to the complete problem are in very good agreement with the results of the first-order analysis, in the present work, attention is focused on the resolution of the multiscaling at order $O(1)$. It should be noted that at this order only the short spatial scale y is of relevance.

In the following, a summary of the most significant transient behavior and asymptotic fate of three-dimensional perturbations is presented to highlight the agreement between
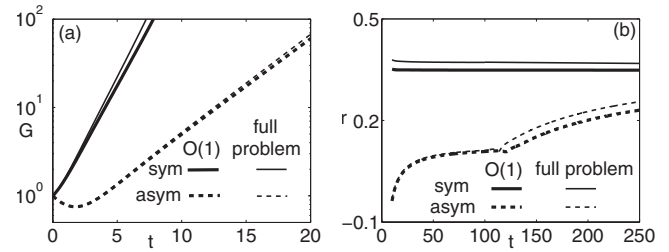

FIG. 6. Transversal long waves. Effect of the symmetry of the perturbation. Comparison between multiscale $O(1)$ (thick curves) and full problem (thin curves). (a) The amplification factor G and (b) the temporal growth rate r as function of time. Re=100, k=0.02, $\phi=\pi/2$, x_0=10, α_i=0.08, symmetric and asymmetric initial conditions.

solutions of multiscaling at order $O(1)$ and full linear problem. Results will be principally focused on parameters such as the spatial damping rate, the polar wave number value (to check the validity of the approximation), the angle of obliquity and the symmetry of the three-dimensional disturbance.

To measure the transient growth the concepts of kinetic-energy density $e(t; k, \phi, \alpha_i)$

$$e(t; k, \phi, \alpha_i) = \frac{1}{2} \frac{1}{2y_d} \int_{-y_d}^{+y_d} (|\hat{u}|^2 + |\hat{v}|^2 + |\hat{w}|^2) dy$$

$$= \frac{1}{2} \frac{1}{2y_d} \frac{1}{|k^2 + 2ik\cos(\phi)\alpha_i - \alpha_i^2|}$$

$$\times \int_{-y_d}^{+y_d} \left(\left| \frac{\partial \hat{v}}{\partial y} \right|^2 + |k^2 + 2ik\cos(\phi)\alpha_i - \alpha_i^2||\hat{v}|^2 + |\hat{\omega}_y|^2 \right) dy, \tag{24}$$

and normalized amplification factor $G(t; k, \phi, \alpha_i)$,

$$G(t; k, \phi, \alpha_i) = \frac{e(t; k, \phi, \alpha_i)}{e(t = 0; k, \phi, \alpha_i)}, \tag{25}$$

are introduced for both multiscale $O(1)$ quantities $(\hat{v}_0, \hat{\Gamma}_0, \hat{\omega}_{y0})$ and full problem quantities $(\hat{v}, \hat{\Gamma}, \hat{\omega}_y)$.

In Eq. (16), the limits $\pm y_d$ define the spatial extension of the numerical domain. The value y_d is defined so that the numerical solutions are insensitive to further extensions of the computational domain size. Here, in the limit of long waves, the size of the spatial domain $2y_d$ assumes values in the range between 30 and 100 external flow scale D. The total kinetic energy can be obtained by integrating the energy density over all k and ϕ.

To evaluate the asymptotic behavior we introduce the temporal growth rate r defined as

$$r(t; k, \phi, \alpha_i) = \frac{\log|e(t; \alpha, \gamma)|}{2t}, \quad t > 0. \tag{26}$$

The temporal growth rate r is not defined for $t=0$. This quantity has, in fact, a precise physical meaning asymptotically in time. Moreover, for both multiscale and the full problem solutions, the angular frequency (pulsation) ω of the pertur-
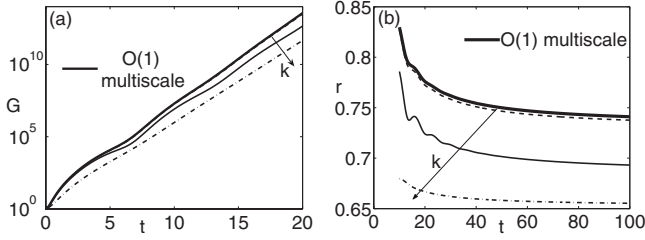
FIG. 7. Effects of the polar wave number k used as small parameter. (a) The amplification factor G and (b) the temporal growth rate r as function of time. Comparison between multiscale $O(1)$ (thick curves) and full problem (thin curves). Re=100, $\phi=0$, x_0 =27, $\alpha_i=0.2$, symmetric initial condition, $k=0.1, 0.01, 0.001$.

bation can be introduced by defining a local, in space and time, time phase φ of the complex wave,

$$\hat{v}(y,t;\alpha,\gamma,\mathrm{Re}) = A_t(y;\alpha,\gamma,\mathrm{Re})e^{i\varphi(t)}, \qquad (27)$$

and then computing the time derivative of the phase perturbation φ,

$$\omega(y,t;k,\phi,\alpha_i) = \frac{d\varphi(y,t;k,\phi,\alpha_i)}{dt}. \qquad (28)$$

Since φ is defined as the phase variation in time of the perturbative wave, it is reasonable to expect constant values of frequency, once the asymptotic state is reached.

III. RESULTS

Computations to evaluate the long time asymptotics are made by integrating the equations forward in time beyond the transient until the temporal growth rate r, defined in relation (26), asymptotes to a constant value ($dr/dt < \epsilon$) [12,22].

Figure 5 presents an interesting phenomenon that is observed for general long perturbations (either transversal or oblique or longitudinal) by changing the value of the spatial damping α_i. For instance, in the case shown in this figure, which is relevant to a long oblique asymmetric wave, the variation in the order of magnitude of α_i from 0.04 to 0.4 highly enhances the amplification in time, with a temporal growth rate that becomes nearly three times larger. This means that perturbations that are spatially confined are more amplified in time. It can also be noted that the agreement between multiscale $O(1)$ (thick curves) and full problem (thin curves) remains very good when changing the order of magnitude of the spatial damping.

The influence of the perturbation symmetry on the early time behavior is shown in Fig. 6 [a logarithmic scale is used on the ordinate of part (a) of the figure]. It can be noted that the symmetric initial condition leads—in the transient behavior—to a faster temporal growth than the asymmetric one, although both configurations are approaching the same asymptotic unstable state. Indeed, the transient in the asymmetric case is lasting longer than $t \sim 10^2$, where in the symmetric case is lasting $t \sim 10^1$. The agreement between multiscale to $O(1)$ and the full problem is very good for both asymmetric and symmetric conditions. This is true both for
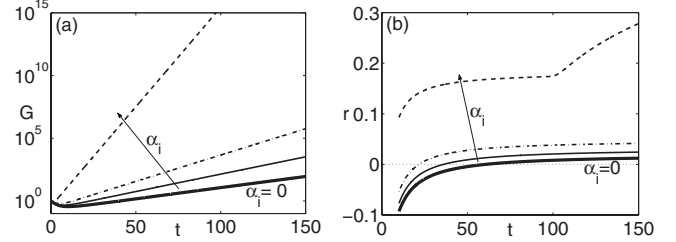
the early transient as well as the ultimate fate. It should be noted the discontinuous behavior shown at $t \sim 100$ by the temporal growth rate of the asymmetric transversal ($\phi = \pi/2$) wave.

The effect of differing orders of magnitude for the polar wave number k is highlighted in Fig. 7. Three orders are considered, namely $k=0.1, 0.01, 0.001$. As expected, for smaller values of the polar wave number the agreement between multiscale $O(1)$ and full problem is improving [the multiscale $O(1)$ solution practically coincides with that of the full problem for $k=0.001$]. It is interesting to note in the interval between zero and 40 base flow time scales, the presence of a temporal oscillation characterized by a period of about ten time scales. The transient thus presents a further time scale beyond its proper global one which, in this case, is lasting 100 units.

The limit for a zero spatial decay, i.e., $\alpha_i \to 0$, was considered in different situations (see Fig. 8) transients of an orthogonal long wave perturbation and (Fig. 9) time asymptotics of an oblique long wave perturbation. In Fig. 8, the thick curves represent the full problem solution with $\alpha_i=0$, while the thin curves are the multiscale $O(1)$ results with α_i values going to zero. The right limit of the multiscale $O(1)$ solution for $\alpha_i \to 0$ is finite and is closely reaching the full problem solution. As can be observed, the curves with smaller spatial decay rates are approaching the thick curve from above. This behavior holds in the early transient and in the asymptotic state. It should be noted that, in this particular

FIG. 8. Transversal long waves. Effect of the spatial decay, α_i. Comparison between multiscale $O(1)$ (thin curves) in the limit for $\alpha_i \to 0$ and full problem (thick curves) with $\alpha_i=0$. (a) The amplification factor G and (b) the temporal growth rate r as function of time. Re=50, $\phi=\pi/2$, $x_0=10$, asymmetric initial condition, $k=0.04$, $\alpha_i=0.005, 0.01, 0.05$ [multiscale $O(1)$], $\alpha_i=0$ (full problem).
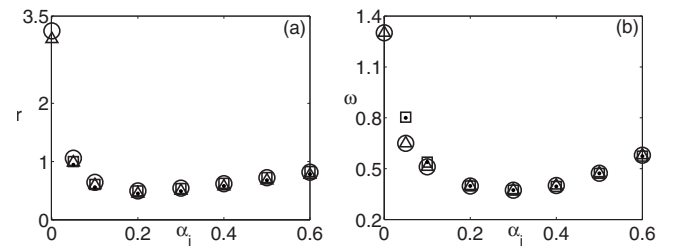

FIG. 9. Temporal asymptotic values of (a) the temporal growth rate and (b) the angular frequency. Comparison between multiscale $O(1)$ (squares: symmetric inputs and dots: asymmetric inputs) and full linear problem (circles: symmetric inputs, triangles: asymmetric inputs). $k=0.01$, Re=100, $\phi=\pi/4$, $x_0=10$, and $dr/dt < \epsilon$ with $\epsilon \sim 10^{-4}$.

case (Re=50, $\phi=\pi/2$, $x_0=10$, asymmetric initial condition, $k=0.04$), the complete problem at $\alpha_i=0$ has a temporal growth rate close to zero and thus is in a near state of marginal stability. But, as previously remarked (cf. Sec. II), this is not a general behavior for the complete problem. However, it is true that the limiting behaviors for $\alpha_i \rightarrow 0$ of the multiscaling and of the complete problem are very close. And, as the case shown in Fig. 6 confirms that, if a difference exists, this will be located just at $\alpha_i=0$. This means that the right limit of the multiscaling for $\alpha_i=0$ correctly approximates the complete problem, but this limit value is not always equal to the value at $\alpha_i=0$ (where the multiscaling yields marginal stability, i.e., $r=0$, $G=1$, and $\omega=0$). It can be concluded that, in any case, the true limit of the complete problem can be obtained by extrapolating the multiscaling results.

It is noted that, in Fig. 8, for asymmetric and transversal initial conditions with a nonvanishing spatial decay, a discontinuity in the temporal growth rate can again be observed at $t \sim 100$, see also Fig. 3.

The comparison between the long waves temporal asymptotics of the full problem and its multiscaling version is shown in Fig. 9. To consider a situation where the multiscaling applies the polar wave number k is fixed to the value 0.01, while the decay in space α_i of the longitudinal wave is in the range [0,0.6]. Multiscale to $O(1)$ results (squares and dots) are in excellent agreement, for symmetric and asymmetric initial inputs, with full problem data (circles and triangles). Note that the agreement improves for increasing values of α_i. A minimum of the perturbation energy (in terms of r) is found around $\alpha_i=0.2-0.3$ and a similar behavior is shown by the angular frequency ω.

IV. CONCLUSIONS

Different transient configurations have been observed by changing the spatial damping rate, the symmetry of the perturbation, and its polar wave number (the magnitude, in order to check the method accuracy, and the angle of obliquity). Since the results relevant to the complete problem are in very good agreement with the results of the first-order analysis, in the present work attention was focused on the resolution of the multiscaling at order $O(1)$ only.

Two main results can be noted. First, the perturbation symmetry influences the transient. In particular, asymmetric transversal perturbations show a different kind of transient which includes an initial decay (first few time scales) and then a growth that abruptly changes its time derivative after about 100 time scales. A sequence of such a kind of discontinuities can be envisaged up to where the growth rate of the corresponding symmetric perturbation is met. Second, the spatial decay substantially affects the transient. For example, in the case of asymmetric perturbations, it is observed that high spatial damping makes the initial temporal decay interval shorter and, at the same time, greatly increases the temporal growth rate.

Multiscale data have been compared with full problem results in the asymptotic temporal limit. As far as small wave numbers are concerned, the agreement is very good for both symmetric and asymmetric initial conditions as arbitrarily expressed in terms of elements of the trigonometrical Schauder basis for the L^2 space.

Lastly, it is noted that the amplification factor of transversal perturbations never presents the trend—a growth followed by a long damping—usually observed in waves with wave number of order one or less. Asymptotically unstable configurations in time have always been observed here in the limit of long waves.

APPENDIX A: BASE FLOW COEFFICIENTS

Here we detail the coefficients, $\phi_i(y;x_0,\text{Re})$ and $\chi_i(y;x_0,\text{Re})$, of the asymptotic expansion representing the intermediate and far base flow. This approximation is homogeneous in the x and z directions and parametrized through the downstream station x_0 and the Reynolds number Re.

1. Zero order: $i=0$

$$\phi_0 = C_0, \tag{A1}$$

$$\chi_0 = 0, \tag{A2}$$

with $C_0=1$.

2. First order: $i=1$

$$\phi_1 = -AC_1 e^{-\text{Re}\, y^2/(4x_0)}, \tag{A3}$$

$$\chi_1 = 0, \tag{A4}$$

with $C_1=1$.

3. Second order: $i=2$

$$\phi_2 = -\frac{1}{2}A^2 e^{-\text{Re}\, y^2/(4x_0)} \left[C_2 \, {}_1\text{F}_1\left(-\frac{1}{2},\frac{1}{2};\frac{\text{Re}\, y^2}{4x_0}\right) \right.$$
$$\left. + e^{-\text{Re}\, y^2/(4x_0)} + \frac{1}{2}\frac{y}{\sqrt{x_0}}\sqrt{\pi\,\text{Re}}\,\text{erf}\left(\frac{1}{2}\sqrt{\frac{\text{Re}}{x_0}}y\right) \right], \tag{A5}$$

$$\chi_2 = -\frac{A}{2}\frac{y}{\sqrt{x_0}}e^{-\text{Re}\, y^2/(4x_0)} \tag{A6}$$

with $C_2=-2.758\,33+0.212\,37\,\text{Re}-0.003\,53\,\text{Re}^2 +0.000\,02\,\text{Re}^3$.

4. Third order: $i=3$

$$\phi_3 = A^3 e^{-\text{Re}\, y^2/(4x_0)}\left(2-\text{Re}\frac{y^2}{x_0}\right)\left[\frac{1}{2}C_3 - \text{Re}\, F_3(x_0,y)\right], \tag{A7}$$

$$\chi_3 = -\frac{A^2}{2}\left\{ C_2\left[-\frac{1}{2}\frac{1}{\sqrt{x_0}} \right.\right.$$

$$\times \int_0^y \left[e^{-\mathrm{Re}\zeta^2/(4x_0)} \, {}_1F_1\left(-\frac{1}{2},\frac{1}{2};\frac{\mathrm{Re}\zeta^2}{4x_0} \right) \right] d\zeta$$

$$\left. -\frac{1}{2}\frac{y}{\sqrt{x_0}}e^{-\mathrm{Re}y^2/(4x_0)} \, {}_1F_1\left(-\frac{1}{2},\frac{1}{2};\frac{\mathrm{Re}y^2}{4x_0} \right) \right]$$

$$-\frac{1}{2}\frac{y}{\sqrt{x_0}}e^{-\mathrm{Re}\,y^2/(2x_0)} - \sqrt{\frac{\pi}{2\,\mathrm{Re}}}\,\mathrm{erf}\left(\sqrt{\frac{\mathrm{Re}}{2x_0}}y \right)$$

$$\left. +\left(\frac{1}{2}\sqrt{\frac{\pi}{\mathrm{Re}}} - \frac{\sqrt{\pi\mathrm{Re}}}{4}\frac{y^2}{x_0} \right)e^{-\mathrm{Re}\,y^2/(4x_0)}\,\mathrm{erf}\left(\frac{1}{2}\sqrt{\frac{\mathrm{Re}}{x_0}}y \right) \right\},$$

$$(A8)$$

with $C_3 = -2.266\,05 + 0.157\,52\,\mathrm{Re} - 0.002\,65\,\mathrm{Re}^2 + 0.000\,01\,\mathrm{Re}^3$.

Coefficient A is related to the drag coefficient C_D [$A = \frac{1}{4}(\mathrm{Re}/\pi)^{1/2}c_D(\mathrm{Re})$], ${}_1F_1$ is the confluent hypergeometric function, $\mathrm{Hr}_{n-1}(\eta) = H_{n-1}(\frac{1}{2}\mathrm{Re}^{1/2}\,\eta)$, where H_n are Hermite polynomials and

$$F_n(\eta) = \int \frac{e^{\mathrm{Re}/2\,\eta^2}}{\mathrm{Hr}_{n-1}^2(\eta)}G_n(\eta)d\eta, \qquad (A9)$$

$$G_n(\eta) = A^{-n}\int M_n(\eta)\mathrm{Hr}_{n-1}(\eta)d\eta, \qquad (A10)$$

where $\eta = y/\sqrt{x_0}$.

APPENDIX B: ORDINARY DIFFERENTIAL OPERATORS OF THE INITIAL-VALUE PROBLEM

In this appendix we list the ordinary differential operators of the full linear system and, up to order $O(k)$, of the multi-scale system. The coefficients inside these operators are the quantities computed in x_0 that are associated to the spatial derivatives of the vorticity and velocity of the base flow $\{\mathbf{U} = [U(y;x_0,\mathrm{Re}), V(y;x_0,\mathrm{Re})]\}$. In particular, $\Omega_z = (\frac{\partial V}{\partial x} - \frac{\partial U}{\partial y})|_{x=x_0}$ is the mean vorticity in the spanwise direction, and the coefficients a, b, c, d, and e are equal to

$$a = \left.\frac{\partial \Omega_z}{\partial x}\right|_{x=x_0}, \quad b = \left.\frac{\partial^2 \Omega_z}{\partial x^2}\right|_{x=x_0}, \quad c(y) = \left.\frac{\partial^2 \Omega_z}{\partial x\,\partial y}\right|_{x=x_0}, \quad d = \left.\frac{\partial U}{\partial x}\right|_{x=x_0}, \quad e = \left.\frac{\partial V}{\partial x}\right|_{x=x_0}.$$

1. Full linear problem

$$G = -i[k\cos(\phi) + i\alpha_i]U - V\frac{\partial}{\partial y} + \frac{1}{\mathrm{Re}}\left[\frac{\partial^2}{\partial y^2} - k^2 + \alpha_i^2 - 2ik\cos(\phi)\alpha_i \right], \qquad (B1)$$

$$H = -\frac{i[k\cos(\phi) + i\alpha_i]}{k^2 + 2ik\cos(\phi)\alpha_i - \alpha_i^2}b\frac{\partial}{\partial y} - c(y) - i[k\cos(\phi) + i\alpha_i]\frac{\partial\Omega_z}{\partial y} + \frac{k^2\cos^2(\phi) + 2ik\cos(\phi)\alpha_i - \alpha_i^2 - k^2\sin^2(\phi)}{k^2 + 2ik\cos(\phi)\alpha_i - \alpha_i^2}$$

$$\times a\frac{\partial}{\partial y} + k^2\sin^2(\phi)\frac{\partial V}{\partial y} + [k^2\cos^2(\phi) + 2ik\cos(\phi)\alpha_i - \alpha_i^2]d - \frac{k^2\cos^2(\phi) + 2ik\cos(\phi)\alpha_i - \alpha_i^2}{k^2 + 2ik\cos(\phi)\alpha_i - \alpha_i^2}d\frac{\partial^2}{\partial y^2}$$

$$-\frac{k^2\sin^2(\phi)}{k^2 + 2ik\cos(\phi)\alpha_i - \alpha_i^2}\frac{\partial V}{\partial y}\frac{\partial^2}{\partial y^2} - i[k\cos(\phi) + i\alpha_i]e\frac{\partial}{\partial y} + \frac{i[k\cos(\phi) + i\alpha_i]}{k^2 + 2ik\cos(\phi)\alpha_i - \alpha_i^2}e\frac{\partial^3}{\partial y^3}, \qquad (B2)$$

$$K = +\frac{k\sin(\phi)}{k^2 + 2ik\cos(\phi)\alpha_i - \alpha_i^2}b - ik\sin(\phi)e - 2\frac{[k\cos(\phi) + i\alpha_i]k\sin(\phi)}{k^2 + 2ik\cos(\phi)\alpha_i - \alpha_i^2}a + \frac{[k\cos(\phi) + i\alpha_i]k\sin(\phi)}{k^2 + 2ik\cos(\phi)\alpha_i - \alpha_i^2}d\frac{\partial}{\partial y}$$

$$-\frac{[k\cos(\phi) + i\alpha_i]k\sin(\phi)}{k^2 + 2ik\cos(\phi)\alpha_i - \alpha_i^2}\frac{\partial V}{\partial y}\frac{\partial}{\partial y} - i\frac{k\sin(\phi)}{k^2 + 2ik\cos(\phi)\alpha_i - \alpha_i^2}e\frac{\partial^2}{\partial y^2}, \qquad (B3)$$

$$L = -i[k\cos(\phi) + i\alpha_i]U - V\frac{\partial}{\partial y} + \frac{1}{\mathrm{Re}}\left[\frac{\partial^2}{\partial y^2} - k^2 + \alpha_i^2 - 2ik\cos(\phi)\alpha_i \right] - d + \frac{i[k\cos(\phi) + i\alpha_i]}{k^2 + 2ik\cos(\phi)\alpha_i - \alpha_i^2}e\frac{\partial}{\partial y}, \qquad (B4)$$

$$M = -ik\sin(\phi)\frac{\partial U}{\partial y} + \frac{ik\sin(\phi)}{k^2 + 2ik\cos(\phi)\alpha_i - \alpha_i^2}e\frac{\partial^2}{\partial y^2}. \qquad (B5)$$

2. Order $O(1)$

$$G_0 = \alpha_i U - V\frac{\partial}{\partial y} + \frac{1}{\text{Re}}\left(\frac{\partial^2}{\partial y^2} + \alpha_i^2\right), \qquad \text{(B6)}$$

$$H_0 = a\frac{\partial}{\partial y} - \frac{1}{\alpha_i}b\frac{\partial}{\partial y} + \alpha_i\frac{\partial\Omega_z}{\partial y} - c(y) - d\left(\alpha_i^2 + \frac{\partial^2}{\partial y^2}\right)$$
$$+ \frac{1}{\alpha_i}\left(\alpha_i^2\frac{\partial}{\partial y} + \frac{\partial^3}{\partial y^3}\right), \qquad \text{(B7)}$$

$$L_0 = \alpha_i U - V\frac{\partial}{\partial y} + \frac{1}{\text{Re}}\left(\frac{\partial^2}{\partial y^2} + \alpha_i^2\right) - d + \frac{1}{\alpha_i}e\frac{\partial}{\partial y}. \quad \text{(B8)}$$

3. Order $O(k)$

$$G_1 = -i\cos(\phi)U - V\frac{\partial}{\partial Y} + \frac{1}{\text{Re}}\left[2\frac{\partial^2}{\partial y\,\partial Y} - 2i\cos(\phi)\alpha_i\right], \qquad \text{(B9)}$$

$$H_1 = a\frac{\partial}{\partial Y} - \frac{1}{\alpha_i}b\frac{\partial}{\partial Y} + -\frac{i}{\alpha_i^2}\cos(\phi)b\frac{\partial}{\partial y} - i\cos(\phi)\frac{\partial\Omega_z}{\partial y}$$
$$-2\frac{\partial^2}{\partial y\,\partial Y}d + 2i\alpha_i\cos(\phi)d + \frac{3}{\alpha_i}\frac{\partial^3}{\partial y^2\,\partial Y}e + \alpha_i e\frac{\partial}{\partial Y}$$
$$+ \frac{i}{\alpha_i^2}\cos(\phi)e\frac{\partial^3}{\partial y^3} - i\cos(\phi)e\frac{\partial}{\partial y},$$

$$K_1 = \frac{2}{\alpha_i}\sin(\phi)a - \frac{i}{\alpha_i^2}\sin(\phi)b + -i\sin(\phi)e\left(1 - \frac{1}{\alpha_i^2}\frac{\partial^2}{\partial y^2}\right), \qquad \text{(B10)}$$

$$L_1 = -i\cos(\phi)U - V\frac{\partial}{\partial Y} + \frac{1}{\text{Re}}\left[2\frac{\partial^2}{\partial y\,\partial Y} - 2i\cos(\phi)\alpha_i\right]$$
$$+ \frac{1}{\alpha_i}e\left(\frac{\partial}{\partial Y} + \frac{i}{\alpha_i}\cos(\phi)\frac{\partial}{\partial y}\right),$$

$$M_1 = -i\sin(\phi)\frac{\partial U}{\partial y} - \frac{i}{\alpha_i^2}\sin(\phi)e\frac{\partial^2}{\partial y^2}. \qquad \text{(B11)}$$

[1] C. E. Grosch and H. Salwen, J. Fluid Mech. **34**, 177 (1968).
[2] H. Salwen and C. E. Grosch, J. Fluid Mech. **104**, 445 (1981).
[3] W. O. Criminale, T. L. Jackson, and R. D. Joslin, *Theory and Computation in Hydrodynamic Stability* (Cambridge University Press, Cambridge, 2003).
[4] P. J. Schmid and D. S. Henningson, *Stability and Transition in Shear Flows* (Springer-Verlag, New York, 2001).
[5] P. G. Drazin and L. N. Howard, J. Fluid Mech. **14**, 257 (1962).
[6] J. J. Healey, Proc. R. Soc. London, Ser. A **462**, 1467 (2006).
[7] I. I. Ryzhkov and V. M. Shevtsova, Phys. Fluids **21**, 014102 (2009).
[8] R. Barros and W. Choi, Stud. Appl. Math. **122**, 325 (2009).
[9] U. Piomelli, T. A. Zang, C. G. Speziale, and M. Y. Hussaini, Phys. Fluids A **2**, 257 (1990).
[10] M. Germano, U. Piomelli, P. Moin, and W. H. Cabot, Phys. Fluids A **3**, 1760 (1991).
[11] W. O. Criminale and P. G. Drazin, Stud. Appl. Math. **83**, 123 (1990).
[12] S. Scarsoglio, D. Tordella, and W. O. Criminale, Stud. Appl. Math. **123**, 153 (2009).
[13] D. Tordella and M. Belan, Phys. Fluids **15**, 1897 (2003).
[14] S. Berrone, Comput. Methods Appl. Mech. Eng. **190**, 4435 (2001).
[15] L. S. G. Kovásznay, Proc. R. Soc. London, Ser. A **198**, 174 (1949).
[16] D. Tordella and S. Scarsoglio, Phys. Lett. A **373**, 1159 (2009).
[17] D. Tordella, S. Scarsoglio, and M. Belan, Phys. Fluids **18**, 054105 (2006).
[18] M. Belan and D. Tordella, J. Fluid Mech. **552**, 127 (2006).
[19] G. I. Barenblatt, *Scaling, Self-similarity, and Intermediate Asymptotics* (Cambridge University Press, Cambridge, 1966).
[20] D. G. Lasseigne, R. D. Joslin, T. L. Jackson, and W. O. Criminale, J. Fluid Mech. **381**, 89 (1999).
[21] S. Scarsoglio, Ph.D. thesis, Politecnico di Torino, 2008.
[22] W. O. Criminale, T. L. Jackson, D. G. Lasseigne, and R. D. Joslin, J. Fluid Mech. **339**, 55 (1997).